The Effect of Various Nanofluids on Absorption Intensification of CO2/SO2 in a Single-Bubble Column

Authors:

Soroush Karamian, Dariush Mowla, Feridun Esmaeilzadeh

Date Submitted: 2019-09-05

Keywords: bubble column, mass transfer coefficient, nanofluids, absorption intensification

Abstract:

Application of nanoparticles in aqueous base-fluids for intensification of absorption rate is an efficient method for absorption progress within the system incorporating bubble-liquid process. In this research, SO2 and CO2 were separately injected as single raising bubbles containing nanofluids to study the impact of nanoparticle effects on acidic gases absorption. In order to do this, comprehensive experimental studies were done. These works also tried to investigate the effect of different nanofluids such as water/Al2O3 or water/Fe2O3 or water/SiO2 on the absorption rate. The results showed that the absorption of CO2 and SO2 in nanofluids significantly increases up to 77 percent in comparison with base fluid. It was also observed that the type of gas molecules and nanoparticles determine the mechanism of mass transfer enhancement by nanofluids. Additionally, our findings indicated that the values of mass transfer coefficient of SO2 in water/Al2O3, water/Fe2O3 and water/SiO2 nanofluids are, respectively, 50%, 42% and 71% more than those of SO2 in pure water (k L SO 2 ? w a t e r = 1.45 × 10 ? 4 m / s). Moreover, the values for CO2 in above nanofluids were, respectively, 117%, 103% and 88% more than those of CO2 in water alone (k L CO 2 ? w a t e r = 1.03 × 10 ? 4 m / s). Finally, this study tries to offer a new comprehensive correlation for mass transfer coefficient and absorption rate prediction.

Record Type: Published Article

Submitted To: LAPSE (Living Archive for Process Systems Engineering)

Citation (overall record, always the latest version): LAPSE:2019.0972
Citation (this specific file, latest version): LAPSE:2019.0972-1
Citation (this specific file, this version): LAPSE:2019.0972-1v1

DOI of Published Version: https://doi.org/10.3390/pr7070393

processes

MDPI

Article

The Effect of Various Nanofluids on Absorption Intensification of CO_2/SO_2 in a Single-Bubble Column

Soroush Karamian [1], Dariush Mowla [2] and Feridun Esmaeilzadeh [2,*]

[1] Department of Chemical Engineering, Shiraz University, Shiraz 7134851154, Iran
[2] Environmental Research Center in Petroleum and Petrochemical Industries, School of Chemical and Petroleum Engineering, Shiraz University, Shiraz 7134851154, Iran
* Correspondence: esmaeil@shirazu.ac.ir

Received: 23 May 2019; Accepted: 21 June 2019; Published: 26 June 2019

Abstract: Application of nanoparticles in aqueous base-fluids for intensification of absorption rate is an efficient method for absorption progress within the system incorporating bubble-liquid process. In this research, SO_2 and CO_2 were separately injected as single raising bubbles containing nanofluids to study the impact of nanoparticle effects on acidic gases absorption. In order to do this, comprehensive experimental studies were done. These works also tried to investigate the effect of different nanofluids such as water/Al_2O_3 or water/Fe_2O_3 or water/SiO_2 on the absorption rate. The results showed that the absorption of CO_2 and SO_2 in nanofluids significantly increases up to 77 percent in comparison with base fluid. It was also observed that the type of gas molecules and nanoparticles determine the mechanism of mass transfer enhancement by nanofluids. Additionally, our findings indicated that the values of mass transfer coefficient of SO_2 in water/Al_2O_3, water/Fe_2O_3 and water/SiO_2 nanofluids are, respectively, 50%, 42% and 71% more than those of SO_2 in pure water ($k_{LSO_2-water} = 1.45 \times 10^{-4}$ m/s). Moreover, the values for CO_2 in above nanofluids were, respectively, 117%, 103% and 88% more than those of CO_2 in water alone ($k_{LCO_2-water} = 1.03 \times 10^{-4}$ m/s). Finally, this study tries to offer a new comprehensive correlation for mass transfer coefficient and absorption rate prediction.

Keywords: nanofluids; absorption intensification; mass transfer coefficient; bubble column

1. Introduction

Combustion of fossil fuels led to deforestation and global warming by the emission of acidic gases such as SO_2 and CO_2 into the environment [1]. Hence, in 1992, the United Nation Conference on Environment and Development offered a new strategy for reducing the emission of acidic and other greenhouse gases to below the standard level until 2000 [1]. Consequently, the governments should finance researchers and scholars to apply new methods and techniques to reduce the amount of CO_2 as well as the SO_2 produced from large-scale industries and sources [2–6].

In order to remove acidic gases from the natural gas, the scrubbing with the amine solution is the main process in the gas refineries. In addition, various techniques including physical and chemical absorption, membrane technology and adsorption methods are applied for the high CO_2/SO_2 production industries such as metal forming plants and petrochemical companies [7–9]. One of new approaches for enhance the absorption process, is addition of nanomaterials to basefluids for obtaining novel solvent with ability to absorb gases efficiently [2,3,10,11]. This method were elucidated by several researchers due to its high efficiency, and it has received much more attention in recent years [12,13].

Krishnamurthy et al. fulfilled a comprehensive research on the application of nanoparticles for increasing of mass transfer rate within a basefluid environment. They revealed that Brownian motion

of nanoparticles, leading to induce the micro-convections in nanofluids, has the most impact on mass transfer rate [14]. Ashrafmansouri et al. comprehensively studied previous research and reported an review to highlight the impacts of nanomaterials in heat and mass transfer processes [11]. They reported that much higher thorough studies are needed to disclose the impacts of main parameters including nanoparticles mean size and morphology on absorption rate by using nanofluids. They also exhibited that nanofluid reusing as well as absorption process modeling are the most important subjects for advancement of this technique. In addition, Kim et al. showed that mass transfer rate of ammonia is enhanced when a few nanoparticles are added to the basefluid. They exhibited that bubbles breaking by nanoparticles considerably enhances mass transfer through increasing interfacial area. They also reported that smaller bubbles were produced in nanofluid than in a base fluid, leading to intensification in mass transfer surface area [15].

Ma et al. declared that by adding CNTs to a basefluid, the localized micro-convection occurs due to the Brownian motion of nanotubes [16]. They reported that induced convection can intensify the ammonia molecular diffusion within the nanofluid. Moreover, they concluded that the grazing effect can be considered another mechanism enhancing the efficiency of NH_3 by means of the bubble absorption process [16]. Absorption of gas molecules by means of the nanoparticle surfaces at the bubble interface and then removing the adsorbed gas components from the nanoparticles surface into the fluid is known as grazing effect [17]. Kang et al. also assessed the impact of Carbon nanotubes on gas absorption in a nanofluid [18]. They also revealed that the mass transfer rate of gaseous ammonia in 0.001 wt. % CNTs loaded in nanofluid was 20% higher than that of pure deionized water [18,19].

Numerous researchers have focused on the application of nanofluids as a potential absorbent for the removal of acidic gases [6,11,12,20–23]. Esmaeili-Faraj et al. exhibited that the removal rate of H_2S enhanced up to 40% when 0.02 wt. % of EGO (Exfoliated Graphene Oxide) is added to deionized water as a basefluid. They showed that the main mechanism for enhanced absorption rate is the grazing effect [4].

Jung et al. performed an extensive research in which Al_2O_3 nanoparticles were scattered in methanol as with nanoparticles volume fractions range of 0.005–0.1 vol. % [24]. They observed that the maximum CO_2 removal was 8.3% at 0.01 vol. % nanoparticles compared to the conditions that pure methanol was used as an absorbent. They concluded that the enhanced CO_2 uptake is due to the mixing effect of Al_2O_3 nanoparticles, which were caused by the particle-laden flows induced by Brownian motion [24]. In addition, they observed that for the concentration above a critical value, insignificant Brownian motion can be seen since the inter-particle interactions declines this motion [24].

Darvanjooghi et al. studied the absorption of CO_2 by means of Fe_3O_4/water nanofluid during the applied alternating and constant magnetic fields [3]. Their results declared that both CO_2 solubility and mass transfer rate are increased when the strength of magnetic field is high. In addition, they found that the solubility of CO_2 and its average molar flux into the nanofluid possess a maximum value by applying an AC magnetic field. Finally, they showed that with the increment of magnetic field strength, the mass diffusivity of carbon dioxide in the nanofluid and renewal surface factor increase, whereas the diffusion layer thickness diminishes.

Although, the impacts of different parameters on gas absorption, by means of nanofluids, are studied in previous works, there are no fully agreement and comprehensive results regarding the influence of nanoparticles types on mass transfer parameters in oxides nanoparticles loaded in nanofluids.

Thus, the aim of this study is to reveal the effect of different metal oxide nanoparticles on SO_2 and CO_2 mass transfer parameters in a single-bubble absorber. Hence, comprehensive experimental studies are done to investigate the molar flux, absorption rate, mass transfer coefficient and diffusivity coefficient. In addition, a new correlation encompassing nanofluid properties was developed in order to estimate mass transfer coefficients of the mentioned gases in nanofluids.

2. Materials and Methods

2.1. Materials

In this research, SiO_2 nanoparticles with the purity of 99.99 wt. %, Al_2O_3 nanoparticles with the purity of 99.98 wt. % and Fe_2O_3 nanoparticles with the purity of 99.92 wt. % were purchased from U.S. Nano Company, United State (see Table 1) to prepare water based nanofluids. In order to perform reverse titration for measuring the quantity of CO_2 and SO_2 dissolved in nanofluids, pure NaOH pellets (99.99 wt. %) and HCl with the purity of 37 vol. % were purchased from Merck Company, Germany. Moreover, phenolphthalein and methyl orange obtained from Merck Company, Germany were used as indicators for determination of the equivalent points. Deionized water was used for the preparation and dilution of nanofluids as well as washing the laboratory glassware. All chemical materials are used as received without further purification.

Table 1. Physical properties of the nanoparticles (NPs) used in this study.

Properties	SiO_2 NPs	Al_2O_3 NPs	Fe_2O_3 NPs
Molecular weight (g/mol)	60.08	101.96	159.69
Density (g/cm^3)	2.196	3.980	5.242
Melting point (°C)	1713	2054	1539
Appearance	White solid powder	White solid powder	Red-brown solid powder

2.2. Apparatus

2.2.1. Nanofluid Preparation Instruments

In this study, the transmission electron microcopy (TEM) and dynamic light scattering (DLS) were used to estimate the size distribution of dry and dispersed metal oxides nanoparticles in deionized water, respectively. The TEM images of SiO_2, Al_2O_3 and Fe_2O_3 nanoparticles were obtained by using Hitachi, 9000 NA, Japan to characterize the size of nanoparticles and their agglomeration [25]. For preparing the sample of nanoparticles used in TEM analysis, a suspension of the nanoparticles dispersed in ethanol (0.001 wt. %) was sonicated by using an ultrasonic bath, Parsonic 30S-400W, 28 kHz, for 20 min and then was placed on the graphite surface. The samples were then put in a vacuum oven to remove the ethanol before being introduced into the TEM test device. DLS, Malvern, Zeta Sizer Nano ZS, United Kingdom, was applied to estimate the sizes of nanoparticles and the size distribution of the obtained metal oxides nanoparticles in deionized water [5,25,26]. The stability and surficial electrostatic charges of the metal oxides nanoparticles in deionized water were estimated by using Zeta Potential test (ELSZ-2000, Otsuka Electronics Co., Osaka, Japan). This analysis is a key indicator of the stability of metal oxides nanoparticles within deionized water [12]. Zeta potential accounts for the electrostatic charges on the surface of nanoparticles causing repulsive forces between dispersed particles. The negatively and positively larger magnitude of zeta potential exhibits a significant stability of nanoparticles in the basefluid, whereas a lower magnitude of maximum Zeta-potential declares the tendency of nanoparticles for agglomeration [27]. A Mass Flow Controller (MFC) model Brooks Instrument 1-888-554-flow, USA, was implemented for the injection of CO_2 and SO_2 gases into the nanofluids through the absorption apparatus. Furthermore, water based nanofluids were prepared by measuring and adding the required weight amounts of metal oxide nanoparticles. To do so, a precise electric balance (TR 120 SNOWREX, Taiwan) was implemented. A pH meter (PCE-PHD 1, PCE-Instruments holding, Southampton, UK) was used for recording the pH of solutions during the titration. Finally, an ultrasonic processor (QSONICA-Q700, NY, USA) was used in order to stop forming the agglomeration of SiO_2, Al_2O_3 and Fe_2O_3 nanoparticles, after they were under a mechanical ball-mill (YKM-2L, Changsha Yonglekang Equipment Co., Changsha, China) for grinding the clustered nanoparticles. A syringe-pump (Viltechmeda Plus SEP21S, manufactured in Vilnius, Lithuania) was

also employed for injection of the titrant to the flask. Lastly, a magnetic stirrer (Model IKA-10038, Staufen, Germany) was used for stirring the solutions.

2.2.2. Experimental Set-Up

The experimental set-up contained a bubble column absorber filled with metal oxide nanoparticles loaded in nanofluids. A certain volume of CO_2 and SO_2 was injected into the nanofluid within the absorption column. Figure 1 exhibits the schematic diagram of a bubble column absorber that consists of a 1 m high and 16.2 mm diameter poly-methyl-meta-acrylate (PMMA) tube used as a semi-batch instrument to examine the absorption of acidic gases by means of nanofluids. In addition, in order to control the rate of gas absorption in nanofluids, a syringe-pump was used for the injection of the aforementioned gases through the absorber column. The gases were continuously injected into nanofluids in the absorber column with the constant flow rate of 500 mL/h in each experiment. The average bubbles diameter ranged from 6.9 to 7 mm, and the time for the rising of bubbles was found to be 2.3 s. Finally, in order to measure the concentration of gases in nanofluids in the reverse titration method, the injection of HCl solution into the discharged nanofluid was performed by means of the syringe-pump.

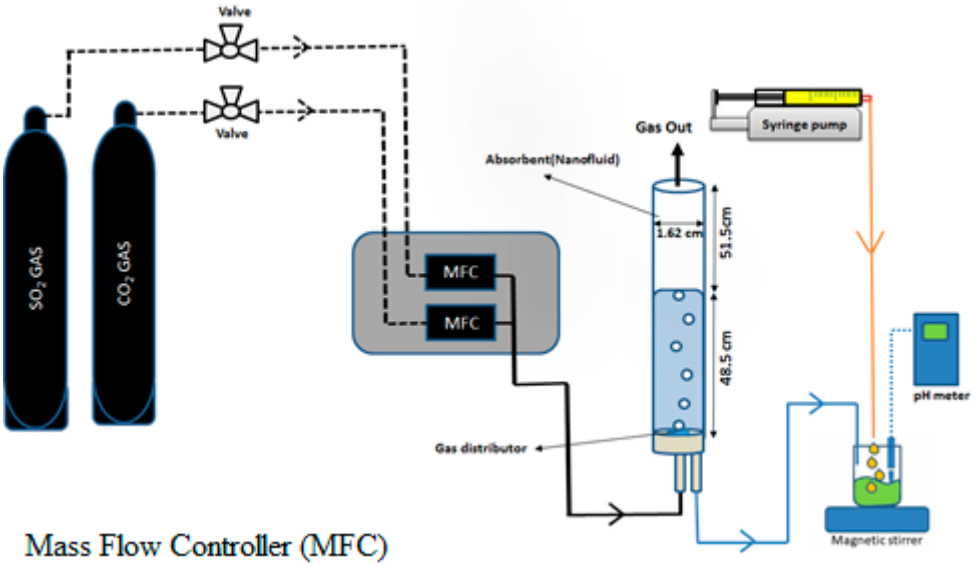

Figure 1. Schematic diagram of experimental set-up.

2.3. Methods

2.3.1. Nanofluid Preparation Procedure

At first, the nanoparticles were introduced to a ball-mill device for about 4 h to separate the agglomeration of nanoparticles. Then, water based nanofluids were prepared with the dispersing of 50 g SiO_2, Al_2O_3 and Fe_2O_3 nanoparticles in 1000 mL deionized water, separately, to produce the main suspension with the nanoparticles concentration of 5.0 wt. %, (equal to 50,000 mg/L). After adding the nanoparticles to deionized water, the suspensions were kept under stirring condition of 800 rpm for 5 h. Finally, the nanoparticles were dispersed in the basefluid by using the sonication process under three sequences of 20 min. The amplitude and cycle time of sonication were set on 70% and 0.5 s, respectively. Also for the preparation of other suspensions with different nanoparticle concentrations of 0.005, 0.01, 0.1, 1.0, and 5.0 wt. %, the stock solutions were diluted with further deionized water.

2.3.2. Experimental Procedure

Sample Analysis Procedure

The analysis for measuring the amounts of absorbed CO_2 and SO_2 in the nanofluids was carried out by using the reverse titration wherein the standard HCl and NaOH solutions were used as the titrant and reactant for producing Na_2CO_3 and Na_2SO_3, respectively [28]. Consequently, in order to determine CO_2 and SO_2 content by using the reverse titration, it is needed to convert H_2SO_3 and H_2CO_3 to Na_2SO_3 and Na_2CO_3, respectively, by the addition of a strong standard base. To do so, the nanofluids were discharged to the flask containing 15 mL of 0.1 M NaOH solution. The carbon dioxide and sulfur dioxide in the solution reacted with the sodium hydroxide and formed sodium bicarbonate or bisulfate as Equation (1) [5]:

$$RO_2 + 2NaOH \rightarrow Na_2RO_3 + H_2O,\ R = C(\text{Carbon}) \quad or \quad S(\text{Sulfur}) \tag{1}$$

The titration was then accomplished to neutralize the amount of remained NaOH, and then excess HCl (as a titrant) in the flask reacted with Na_2SO_3 and Na_2CO_3 during the titration according to the following reactions:

$$Na_2RO_3 + HCl \rightarrow NaCl + NaHRO_3,\ R = C(\text{Carbon}) \quad or \quad S(\text{Sulfur}) \tag{2}$$

$$NaHRO_3 + HCl \rightarrow NaCl + H_2O + RO_2,\ R = C(\text{Carbon}) \quad or \quad S(\text{Sulfur}) \tag{3}$$

According to Equation (2), the discharged samples were titrated with the standard acid solution, (0.1 M HCl), at first equivalent point. The titration with HCl then converted all the remained bicarbonate and bisulfate to SO_2 and CO_2 according to Equation (3). In this method, the difference of consumed HCl between two equivalent points represents the amount of CO_2 or SO_2 absorbed in the solution. Equation (4) was used for determining the value of absorbed gases by means of nanofluids [2,3,28]:

$$C_{RO_2} = \frac{(V_2 - V_1) \times M}{V} \times 10^3 \tag{4}$$

where C_{RO_2} is the absorbed CO_2 or SO_2 concentration in the nanofluids or deionized water (mol/m^3), M is HCl molarity (mol/lit), and V is the volume of absorbent used in the column, (equal to 100 mL), in all experiments. V_1 and V_2 are the volumes (mL) of standard acid solution consumed for neutralizing bicarbonate and bisulfate to SO_2 and CO_2 at two equivalent points, respectively (Figures 2 and 3).

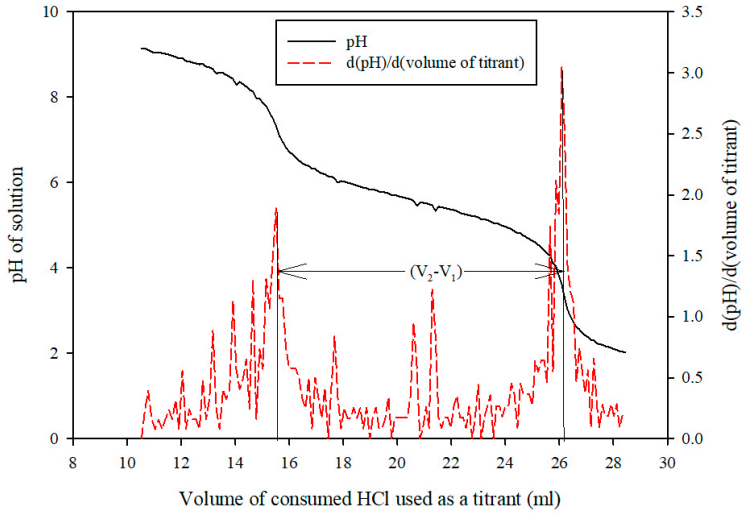

Figure 2. Plot of pH and its differentiation versus volume of consumed titrant, (HCl), for the injection of 50 mL SO_2 through deionized water.

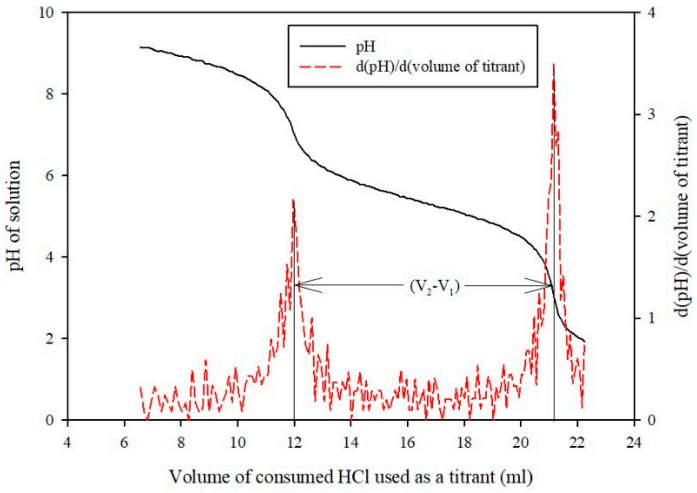

Figure 3. Plot of pH and its differentiation versus volume of consumed titrant, (HCl), for the injection of 50 mL CO_2 through deionized water.

In this work, the molar flux of absorbed CO_2 and SO_2 was calculated by means of the CO_2 and SO_2 concentration in the nanofluid according to the following equation (Equation (5)) [2,3,28]:

$$N_{ave,\,RO_2} = \frac{C_{RO_2} \times V}{(4\pi r_0^2 n) \times (\tau)} \times 10^{-6} \quad (5)$$

Here, N_{ave,RO_2} is the average molar flux transferred from gas, (pure CO_2 or SO_2), to liquid phase (mol/m^2 s), τ is the total gas-liquid contact time of bubbles passing through the nanofluids (s), which is equal to multiply of the bubbles number by raising time of one single bubble (2.3 S), n is the number of bubbles passes through nanofluids within the absorber column and r_0 is the average bubbles radius (3.5 mm) that assumed to be constant at all experiments.

Measurement of Mass Transfer Parameters

In order to obtain the mass transfer coefficient and diffusivity of CO_2 or SO_2 in a water based nanofluid, a set of experiments were performed in which the aforementioned gases were separately injected at the bottom of the column within the volumes of 20, 25, 30, 35, 40, 45 and 50 mL. The mass transfer parameters were then calculated by obtaining the absorption of CO_2 and SO_2 as well as the implementation of the model suggested by Zhao et al. [29].

Uncertainty Analysis

In this research, the uncertainty of the experimentations was calculated by the errors of measurements for parameters, incorporating time of raising bubbles, volume of liquid for the titration method and pH of solutions. The time of raising bubbles was measured by using a digital chronometer with the maximum accuracy of ±0.01 s, the pH of discharged nanofluids was measured during the titration by a pH meter with the maximum accuracy of ±0.1, and the volumes of liquids were measured by laboratories glassware with the maximum accuracy of ±0.1. According to the literature [2,3], the relative uncertainty of final experimental results was calculated as follows [30,31]:

$$U = \pm\sqrt{\left(\frac{\Delta V}{V}\right)^2 + \left(\frac{\Delta t}{t}\right)^2 + \left(\frac{\Delta pH}{PH}\right)^2} \quad (6)$$

Consequently, by substituting the values in Equation (6) the relative uncertainty of the experimental results was found to be less than 5.2 %.

3. Results and Discussion

3.1. Nanofluid Characterization

Figure 4 exhibits the TEM images of SiO_2, Al_2O_3 and Fe_2O_3 nanoparticles that used for the preparation of water based nanofluids. These images show that the diameter of SiO_2 nanoparticles ranged from 20 to 60 nm (Figure 4a), the diameter of Al_2O_3 nanoparticles ranged from 30 to 80 nm (Figure 4b) and the diameter of Fe_2O_3 nanoparticles ranged from 20 to 60 nm (Figure 4c). In addition, the results presented in Figure 4 exhibit that all metal oxides nanoparticles have a semi-spherical morphology that no considerable agglomeration was observed [32].

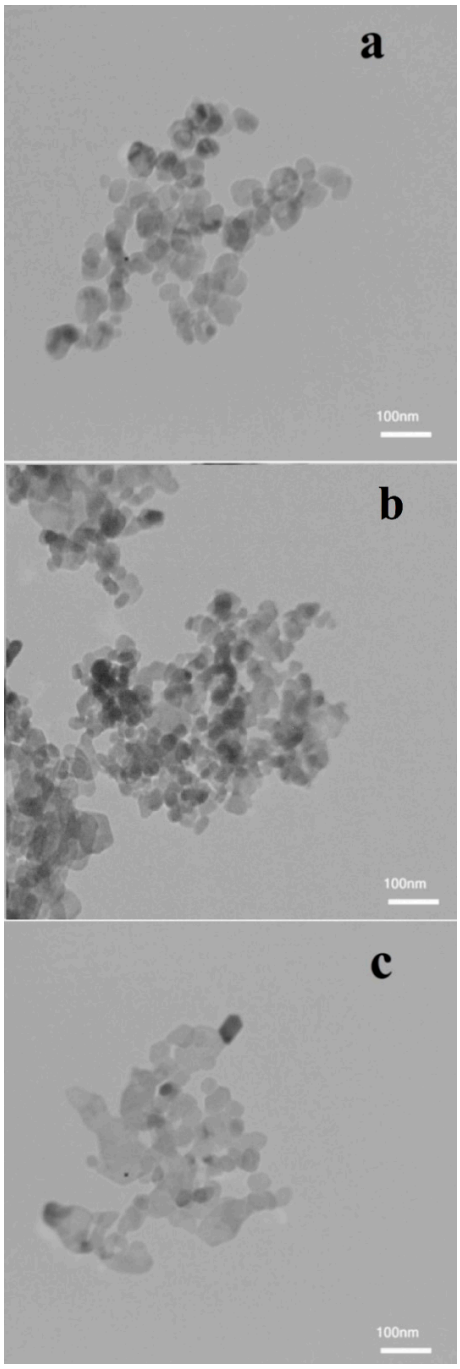

Figure 4. Transmission electron microcopy (TEM) images of (**a**) SiO_2, (**b**) Al_2O_3 and (**c**) Fe_2O_3 nanoparticles.

The results of DLS analysis for SiO_2, Al_2O_3 and Fe_2O_3 nanoparticles dispersed in deionized water exhibited that the mean diameter of nanoparticles for SiO_2 is 48.3 nm with Poly Dispersity Index, (P.D.I.), of 0.105 and the mean diameter of nanoparticles for Al_2O_3 and Fe_2O_3 is found to be 54.7 nm and 55.1 nm, respectively, with P.D.I.s of 0.145 and 0.138, respectively. These results confirm that the dispersion technique, which was used in this research, led to the well-dispersed nanoparticles diameter, with a narrow range of 48.3 to 55.1 nm. The results of this test indicate that the average size of nanoparticles is equal to that estimated by using TEM test declaring no significant agglomeration during the dispersion of nanoparticles in the basefluid.

Zeta-potential analysis can be implemented in order to quantify the stability of nanoparticles in the basefluid [33]. These results represent that nanofluids have high stability due to the fact that their zeta potential is lower than −45 mV [34]. In other words, the magnitude of the zeta potential determines the degree of electrostatic repulsion between similarly charged particles in colloidal dispersions. The large magnitude of the zeta potential for SiO_2/water, Al_2O_3/water and Fe_2O_3/water nanofluids (−97.8 mV for Al_2O_3/water, 100.2 mV for SiO_2/water and 79.5 mV for Fe_2O_3/water nanofluids) indicated high stability of nanoparticles representing high repulsive electrostatic forces [35].

3.2. Absorption

3.2.1. Maximum Absorption

Figure 5 shows the average molar flux of CO_2 into each of these three nanofluids: SiO_2/water, Al_2O_3/water or Fe_2O_3/water. The mass fraction of each metal oxides nanoparticle varies from 0.005 to 5 wt. %. The experimentations were repeated four times at a fixed mass fraction of metal oxides nanoparticles and the standard deviations are shown in this figure as the error bars. According to the results presented in this figure, the average molar flux of CO_2 increases about 21% with the increase of Al_2O_3 nanoparticles from 0.005 to 0.1 wt. % while the molar flux decreases for higher Al_2O_3 nanoparticles loads (0.1 to 5 wt. %). Moreover, the value of CO_2 molar flux increases about 45% when the mass fraction of SiO_2 nanoparticles increases from 0.005 to 0.01 wt. %. Moreover, for higher mass fractions of SiO_2 nanoparticles, a remarkable declination on CO_2 molar flux resulted. In addition, the value of CO_2 molar flux enhances about 16% when mass fraction of Fe_2O_3 nanoparticles enhances from 0.005 to 1 wt. %, and a declination of CO_2 molar flux resulted in the mass fraction range of up to 5 wt. %. Table 2 represents the mass fraction of nanoparticles where by the maximum value of CO_2 molar flux obtained. It can be concluded from this table that CO_2 absorption molar flux has a maximum value at 0.1, 0.01 and 1 wt. % for Al_2O_3/water, SiO_2/water and Fe_2O_3/water nanofluids, respectively. For all nanoparticles types, the nanoparticles intensify the micro-convections, producing larger mass transfer rate in comparison to pure basefluid; thus, initial increase in CO_2 absorption would be rationalizable with the aforementioned nanoparticles mass fractions. On the other hands, increasing a number of nanoparticles leads to enhance further the viscosity of nanofluids, thereby overcoming the nanoparticles micro-convection impacts together with diminishing the absorption of CO_2 within the nanofluids [4,12]. Furthermore, Figure 5 clearly exhibits that CO_2 absorption molar flux in metal oxides-based nanofluids is larger than that in deionized water for various nanoparticles mass loads.

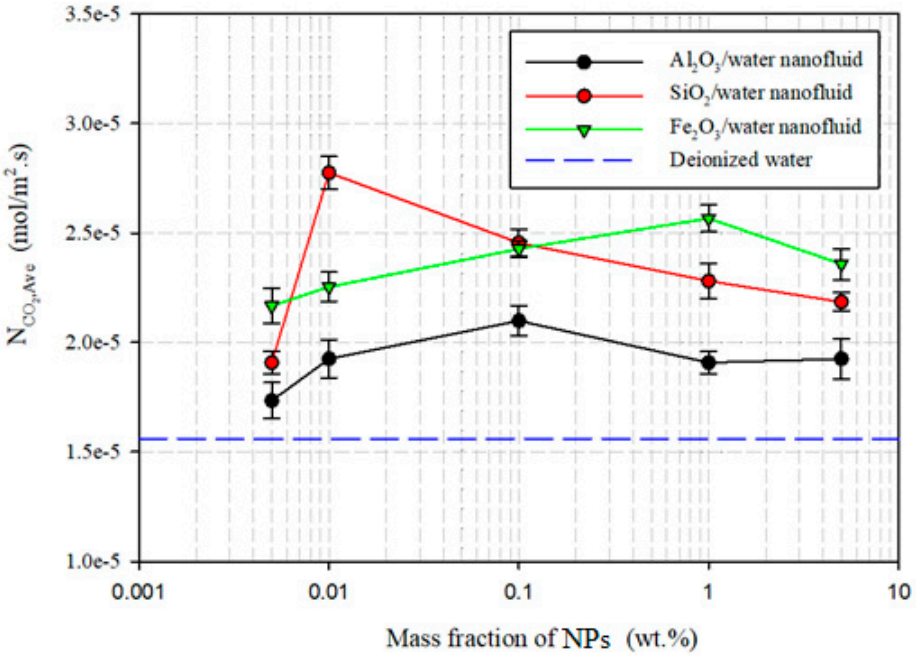

Figure 5. Average molar flux of CO_2 versus mass fraction of metal oxides nanoparticles (NPs).

Table 2. Maximum molar flux and relative absorption rate for SO_2 and CO_2.

Absorbent	SO_2 Absorption			CO_2 Absorption		
	% wt. NPs in N_{max}	N_{max}	$\frac{N_{nf}}{N_{bf}}$	% wt. NPs in N_{max}	N_{max}	$\frac{N_{nf}}{N_{bf}}$
Water (bf)		1.871×10^{-5}	1.000		1.566×10^{-5}	1.000
SiO_2/water	1.0	2.983×10^{-5}	1.594	0.01	2.774×10^{-5}	1.771
Al_2O_3/water	0.1	2.445×10^{-5}	1.307	0.1	2.098×10^{-5}	1.340
Fe_2O_3/water	0.1	3.312×10^{-5}	1.770	1.0	2.566×10^{-5}	1.638

Figure 6 displays the average molar flux of SO_2 into each of these three nanofluids: SiO_2/water, Al_2O_3/water or Fe_2O_3/water. The aforementioned metal oxides nanoparticles were dispersed in deionized water with different concentrations of 0.005, 0.01, 0.1, 1 and 5 wt. %. These experimentations were also repeated four times at a fixed mass fraction of each metal oxide nanoparticle, and the error bars express the standard deviation obtained from the measurements. According to the obtained results, the average molar flux of SO_2 enhances about 28% with the Al_2O_3 nanoparticles enhancement from 0.005 to 0.1 wt. %, and for higher nanoparticles loads, a substantial decrease resulted in its molar flux. In addition, the value of SO_2 absorption rate into SiO_2/water nanofluid increases about 32% when the mass fraction of SiO_2 nanoparticles in deionized water increases from 0.005 to 1 wt. %. After a further increase of mass fraction up to 5 wt. %, the absorption of CO_2 declines. Moreover, the value of CO_2 molar flux increases about 26% when mass fraction of Fe_2O_3 nanoparticles increases from 0.005 to 0.1 wt. %; and with a further increase of nanoparticles mass fraction from 0.1 to 5 wt. %, the value of CO_2 absorption declines. According to the results presented in Table 2, the maximum molar flux of SO_2 can be obtained with the nanoparticles mass fractions of 0.1, 1 and 0.1 wt. % for Al_2O_3/water, SiO_2/water and Fe_2O_3/water nanofluids, respectively. Similar to the results achieved for CO_2 absorption, the addition of nanoparticles into the deionized water enhances the micro-convections and intensifies the mass transfer rate of SO_2 while increasing the nanoparticles load increases further the viscosity of nanofluids, declining the absorption rate of SO_2 into the nanofluids [4,12]. The results presented in this figure show that SO_2 absorption in metal oxides nanofluids is more than that in deionized water.

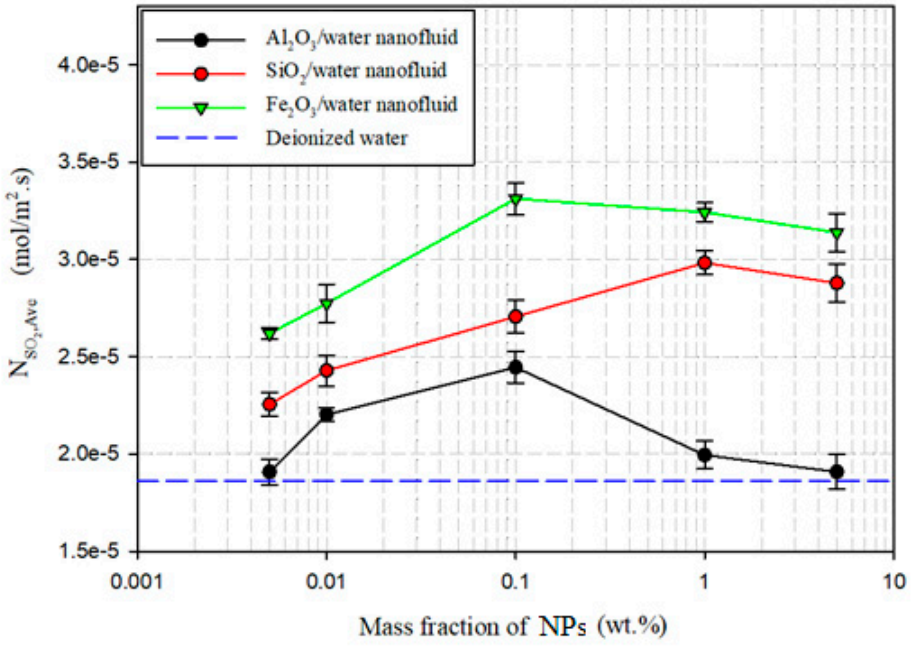

Figure 6. Average molar flux of SO_2 versus mass fraction of metal oxides nanoparticles.

3.2.2. Probing of Mass Transfer Rate

Volume loading rate (mL/mL s), can be attributed to the rate of gas injection divided to the total volume of gas equal to which is 50 mL. It actually represents the time which is passing during the mass transfer process and clearly shows what portion of gas is injected through the nanofluid. Therefore, this parameter can easily show the ability of nanofluid to absorb gas at the beginning of the injection or at the end of the process. Figure 7 presents the results of average CO_2 absorption in each of these three nanofluids: SiO_2/water, Al_2O_3/water or Fe_2O_3/water against the volume loading rate that was measured at the temperature of 25 °C and the optimum mass fractions of 0.1, 0.01 and 1 wt. % for SiO_2, Al_2O_3 and Fe_2O_3 nanoparticles in deionized water, respectively. These findings reveal that the absorption rate increases with the enhancement in volume loading rate. Additionally, it is chiefly clear when Fe_2O_3/water is used as an absorbent, the maximum value of absorption rate is obtained at any volume loading rate. Moreover, these results indicate that the minimum value of CO_2 absorption for the Al_2O_3/water nanofluid resulted in comparison to the other nanofluids assessed in this work. These findings indicated that type of the used nanoparticles had a major effect on mass transfer rate. In addition, it can be concluded from this figure that the mass transfer flux is low at lower volume loading rates, and it increases with the increment of loading rate due to having a higher driving force of mass transfer.

Figure 8 also shows the results of average SO_2 absorption in each of these three nanofluids: SiO_2/water, Al_2O_3/water or Fe_2O_3/water against the volume loading rate that was measured at the temperature of 25 °C and the concentrations of 0.1, 1 and 0.1 wt. % for Al_2O_3, SiO_2 and Fe_2O_3 nanoparticles in deionized water, respectively. These results, which are similar to those obtained for CO_2 absorption, show that the absorption rate increases with the growth in volume loading rate, and when SiO_2/water is used as an absorbent, the maximum value of absorption rate is obtained at each gas volume loading rate; while for CO_2 absorption by using Fe_2O_3/water nanofluid, a higher absorption rate achieved. In addition, it is chiefly evident that the minimum value of SO_2 absorption for the Al_2O_3/water nanofluid resulted in comparison to the other nanofluids assessed in this work, that is similar to CO_2 case. These findings declared that type of the used nanoparticles and their interactions with CO_2 and SO_2 had a major effect on mass transfer rate of the gas into the nanofluids. Moreover, the value of absorption rate is similar to the case of CO_2 absorption.

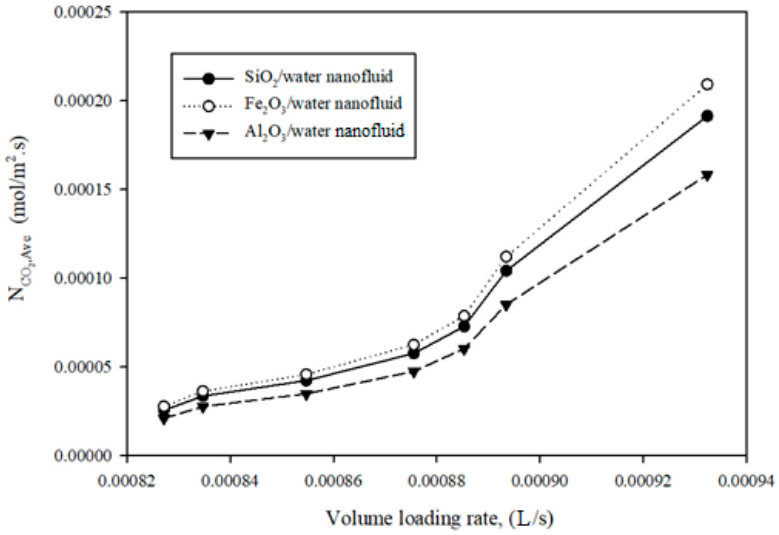

Figure 7. Average molar flux of CO_2 versus volume loading rate.

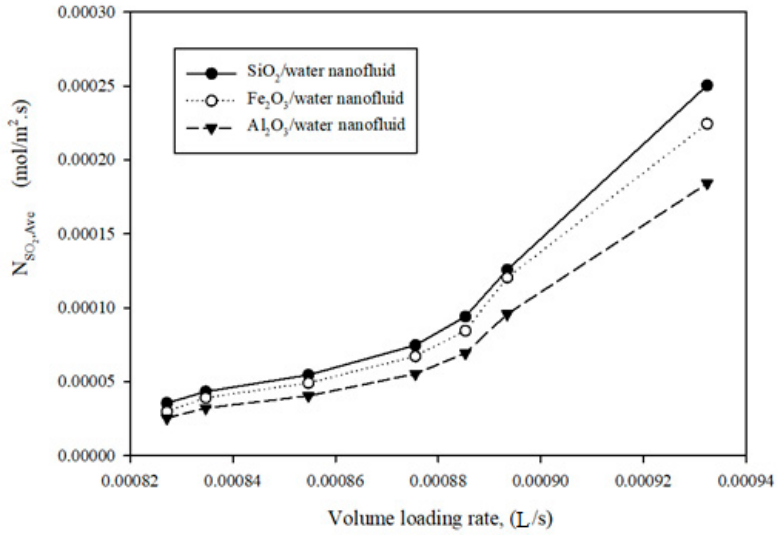

Figure 8. Average molar flux of SO_2 versus volume loading rate.

3.2.3. Mass Transfer Coefficient

For the calculation of mass transfer coefficient, in separate runs, various volumes of gases (20, 25, 30, 35, 40, 45 and 50 mL that are, respectively, equal to 7, 10, 12, 13, 15.6, 17.6 and 20 min total gas-liquid contact time) were injected into the column and then gas concentration and molar flux were measured. Figure 9 shows the average molar flux of CO_2/SO_2 against the dissolved concentration of CO_2/SO_2 in the liquid bulk. These results clearly exhibit that an increase in CO_2/SO_2 bulk concentration consecutively decreases the average value of molar flux due to the reduction of mass transfer driving force. Moreover this observation has approximately a linear behavior for all cases. In order to potpourri of this linear behavior, the principal mass transfer equation (Equation (7)) was used, and the experimental values for the absorption of CO_2/SO_2 by using different nanofluids were fitted to Equation (7):

$$N_{Avg} = k_L\left(C^*_{RO_2,Observed} - C_{RO_2}\right) \quad (7)$$

where k_L is the mass transfer coefficient at liquid phase, (m/s), C_{RO_2} is the bulk concentration of CO_2/SO_2 within the nanofluids, and $C^*_{RO_2,Observed}$ is the observed concentration of CO_2/SO_2 at gas-liquid interface, (mol/m^3). It is mentioned that observed value for gas concentration in the interface was calculated

from extrapolation of line fitted on experimental data. Since linear pattern was assumed for molar flux and gas concentration. According to the results obtained for the absorption of CO_2 into each of these three nanofluids: SiO_2/water, Al_2O_3/water or Fe_2O_3/water (Figure 9a–c), the model was fitted to the experimental data with the R^2 equal to 0.9753, 0.9755 and 0.9897 declaring high accuracy of the regression analysis and low deviation of the experimental data from the fitted model.

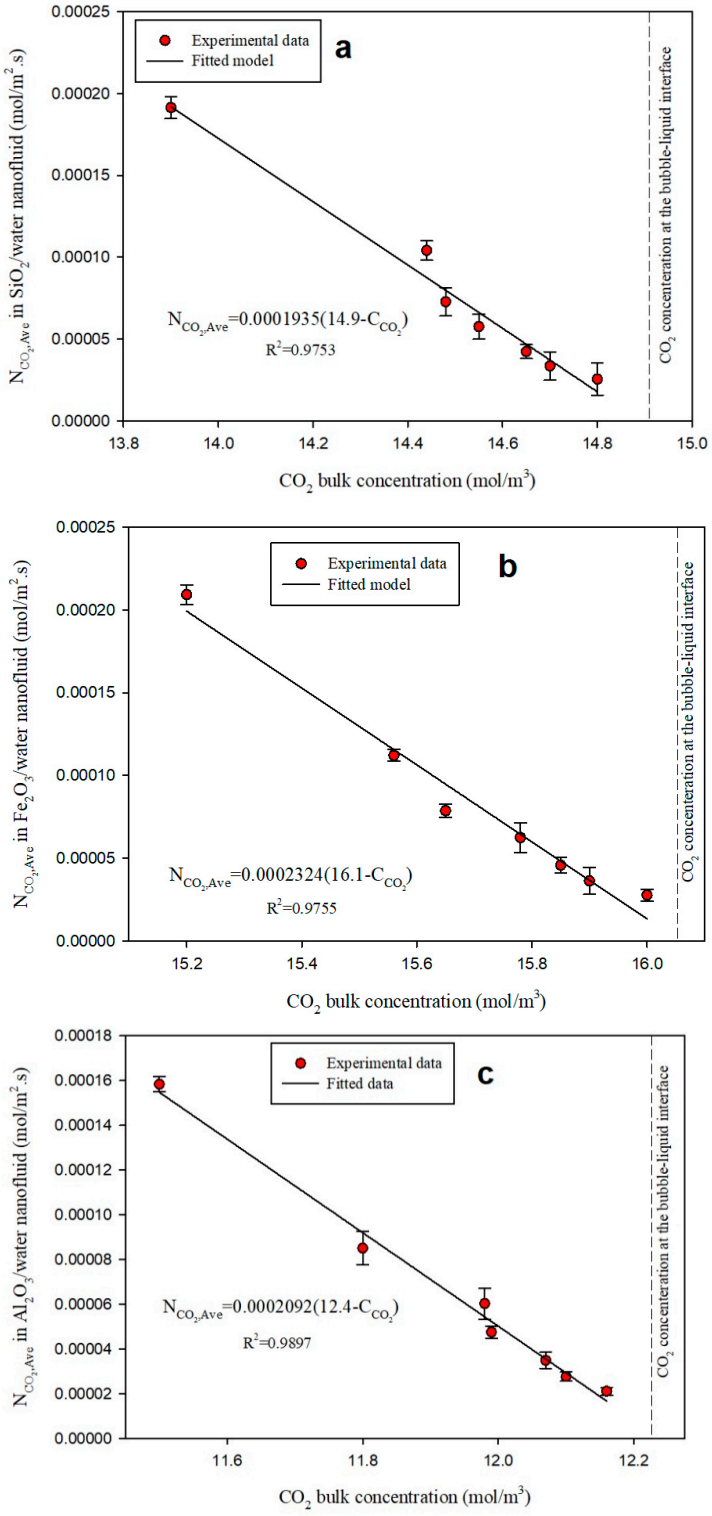

Figure 9. Average molar flux versus CO_2 bulk concentration for (**a**) SiO_2/water, (**b**) Al_2O_3/water and (**c**) Fe_2O_3/water nanofluids.

The average molar flux of SO_2 versus the bulk concentration is shown in Figure 10. These results are also similar to those obtained for CO_2 absorption declaring that an increase in SO_2 bulk concentration leads to decrease the average value of molar flux, representing a significant declination in mass transfer driving force. In order to obtain the mass transfer coefficient and SO_2 concentration at the bubbles-liquid interface, the regression analysis was also performed on Equation (7), and the equation was fitted to the values for SO_2 absorption into each of these three nanofluids: SiO_2/water, Al_2O_3/water or Fe_2O_3/water (Figure 10a–c) with the R^2 equal to 0.9711, 0.9705 and 0.9788, respectively. These values confirm the high accuracy of the regression analysis.

According to the results obtained from Figures 9 and 10, it can be concluded that for all nanofluids used in this study, the vertical diagram (dashed line) shows the observed concentration of CO_2 and SO_2 at the bubble-liquid interface. Furthermore, the diagonal plot of average molar flux versus the bulk concentration of CO_2 and SO_2 represents the operating line for gas absorption into the nanofluids. It is clearly evident that by approaching the operating line to the equilibrium concentration of CO_2 and SO_2 in each of these three nanofluids, namely SiO_2/water, Al_2O_3/water or Fe_2O_3/water, a lower molar flux resulted.

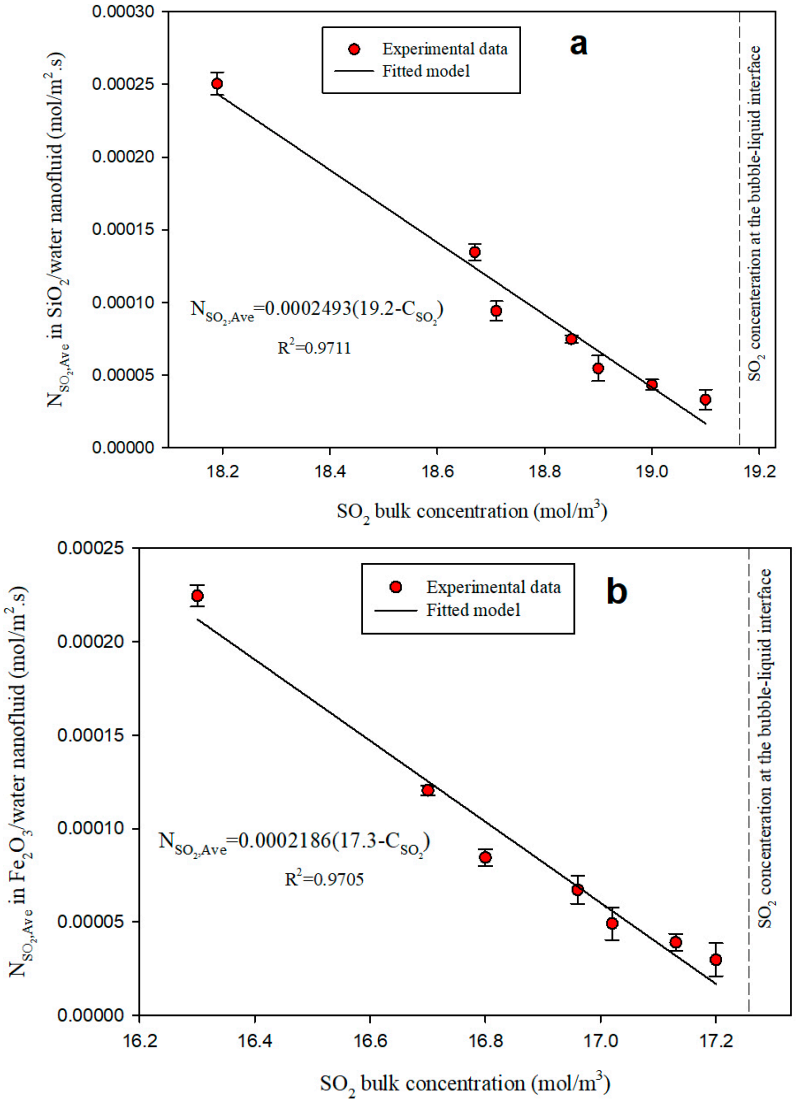

Figure 10. *Cont.*

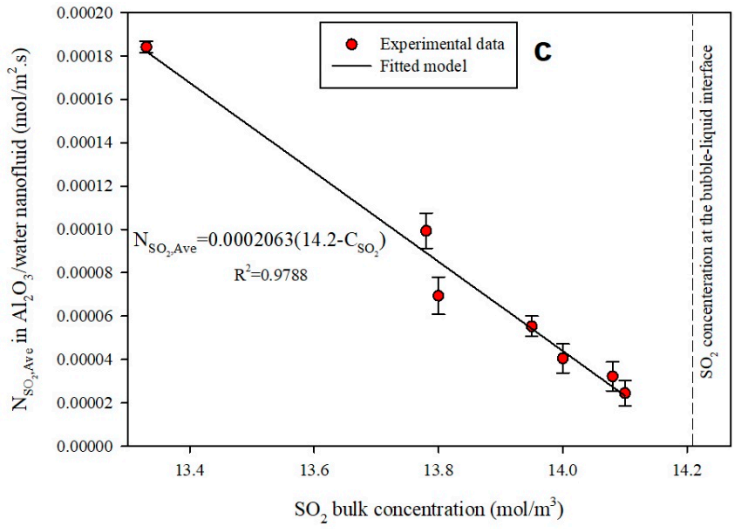

Figure 10. Average molar flux versus SO_2 bulk concentration for (**a**) SiO_2/water, (**b**) Al_2O_3/water and (**c**) Fe_2O_3/water nanofluids.

Table 3 represents the values of relative mass transfer coefficient for SO_2 and CO_2 absorption by using SiO_2/water, Al_2O_3/water or Fe_2O_3/water nanofluids with respect to water alone. These values are the slope of operating line in Figures 9 and 10. According to these results, the maximum value of relative mass transfer coefficient for CO_2 absorption was achieved by Al_2O_3/water nanofluid while the value of relative mass transfer coefficient for SiO_2/water was observed to possess a minimum value in comparison to the other nanofluids assessed in this work. Additionally, these findings exhibit that the maximum value of mass transfer coefficient for SO_2 absorption was achieved for SiO_2/water, and this parameter for Fe_2O_3/water was found to be less than the others. According to the results presented in this table, relative mass transfer coefficient intensively depend on type of the nanofluid. In fact, the absorption of SO_2 by SiO_2/water nanofluid and the absorption of CO_2 by Fe_2O_3/water nanofluid demonstrate higher values for the relative mass transfer coefficient and relative gas concentration at the bubble-liquid interface.

Table 3. Relative mass transfer coefficient for CO_2 and SO_2 in the base fluid (BF) and various nanofluids (NF).

Gas	Absorbent	$k_L \times 10^4$, (m/s)	$\frac{k_{L_{nf}}}{k_{L_{bf}}}$
CO_2	Water (BF)	1.030	1.00
	Water/SiO_2 NF	1.935	1.88
	Water/Fe_2O_3 NF	2.324	2.03
	Water/Al_2O_3 NF	2.092	2.17
SO_2	Water (BF)	1.450	1.00
	Water/SiO_2 NF	2.493	1.71
	Water/Fe_2O_3 NF	2.186	1.42
	Water/Al_2O_3 NF	2.063	1.50

3.3. Diffusivity Coefficient

In general, diffusivity of gases into a fluid has a higher impact on mass transfer coefficient as well as rate of gas absorption. In this study, Equation (8) was used to obtain the diffusivity of SO_2 and CO_2 into each of these three nanofluids, namely SiO_2/water, Al_2O_3/water or Fe_2O_3/water. This equation

indicates a bubble-liquid mass transfer model for raising a single bubble through a liquid based on Dankwert's theory [5,29].

$$N_{Ave} = \frac{D\ sinh\left(\delta\sqrt{\frac{s}{D}}\right) + D\ r_0\ \sqrt{\frac{s}{D}}\ cosh\left(\delta\sqrt{\frac{s}{D}}\right)}{r_0\ sinh\left(\delta\sqrt{\frac{s}{D}}\right)}\left(C_{RO_2,i} - C_{RO_2}\right) \quad (8)$$

In this model, the main factors affecting on mass transfer rate are the surface renewal rate (s), bubbles radius (r_0), diffusion layer thickness (δ) and the diffusivity of gases through a liquid (D). N_{Ave} is the molar flux $\left(mol/m^2\ s\right)$, C_{RO_2} and $C_{RO_2,i}$ are the concentration of dioxide gases within the liquid bulk and at the bubble-liquid interface (mol/m^3), respectively.

By comparing Equations (7) and (8), the mass transfer coefficient of a gas into the liquid by using a single bubble can be obtained from the following relation:

$$k_L = \frac{D\ sinh\left(\delta\sqrt{\frac{s}{D}}\right) + D\ r_0\sqrt{\frac{s}{D}}\ cosh\left(\delta\sqrt{\frac{s}{D}}\right)}{r_0\ sinh\left(\delta\sqrt{\frac{s}{D}}\right)} \quad (9)$$

This equation was used for estimating the diffusivity of SO_2 and CO_2 within the nanofluids. It has been reported by Darvanjooghi et al. that the effective parameters in Equation (9) (s, δ and D) intensively depend on the size of nanoparticles in the basefluid. They reported that the size of nanoparticles was about 40 to 50 nm, and the values of surface renewal rate, s, and the diffusion layer thickness, δ, were 6.85 and 0.201 mm, respectively [2]. In this research, the average mean diameter of nanoparticles ranges from 40 to 60 nm. Additionally, it can be assumed that the values of s and δ would be constant during the absorption of SO_2 and CO_2 and depend on just nanoparticles mean diameter. Additionally, the mass transfer coefficients for both SO_2 and CO_2 gases within the nanofluids studied here have been already calculated in Table 3. Therefore, Equation (9) can be simplified to the following relation:

$$F(D,s,\delta) = \exp\left(2\delta\sqrt{\frac{s}{D}}\right) \mp \frac{D - r_0\sqrt{s.D} - r_0 k_L}{r_0\sqrt{s.D} - r_0 k_L} = 0,\ s = 6.85\ \text{ and } \delta = 0.201 \quad (10)$$

where $F(D,s,\delta)$ must be equal to zero for certain values of mass transfer coefficient and gas diffusivity within the different nanofluids. By using the Newton-Raphson method, Equation 10 can be solved according to the following equation in which $\partial F(D_n,s,\delta)/\partial D_n$ can be obtained by obtaining partial derivative of Equation (10). The initial value of diffusivity, D_0, was set on 10^{-10}.

$$D_{n+1} = D_n - \frac{F(D_n,s,\delta)}{\partial F(D_n,s,\delta)/\partial D_n},\ n = 0,\ 1,\ 2,\ 3,\ldots \quad (11)$$

Table 4 presents the values of SO_2 and CO_2 diffusivities into SiO_2/water, Al_2O_3/water or Fe_2O_3/water nanofluids. According to the results obtained from Table 4, it is evident that the maximum value of diffusivity for the absorption of CO_2 is obtained when water/Fe_2O_3 is used as an absorbent, and the maximum diffusivity for the absorption of SO_2 is achieved when being used water/SiO_2 nanofluid. As can be seen in this table, for nanoparticles with the higher density (ρ_{SiO2} = 2.196 g/cm^3, ρ_{Al2O3} = 3.980 g/cm^3, ρ_{Fe2O3} = 5.242 g/cm^3) more diffusivity of CO_2 within the nanofluid is observed which is attributed to the nanoparticles Brownian motion inducing more diffusion of CO_2 molecules at the bubble-liquid interface. It has been previously reported by Attari et al. that the momentum caused by Brownian velocity of nanoparticles leading to produce micro-convections, depending on nanoparticles density according to the following relation [20]:

$$Mo_{Brownian} = \lambda\sqrt{\rho_p} \quad (12)$$

Table 4. Diffusion coefficient as well as *Re*, *Sh* and *Sc* for CO_2 and SO_2 absorption by using of nanofluids.

Gas	Absorbent	D, (m^2/s)	ν (m/s)	*Sc*	Re_b	*Sh.*
CO_2	Water/SiO_2	5.38×10^{-9}	8.899×10^{-7}	165	1298	234
	Water/Fe_2O_3	7.76×10^{-9}	8.864×10^{-7}	114	1303	195
	Water/Al_2O_3	6.28×10^{-9}	8.451×10^{-7}	135	1367	217
	Deionized water	2.12×10^{-9}	8.900×10^{-7}	420	1298	316
SO_2	Water/SiO_2	8.89×10^{-9}	8.706×10^{-7}	98	1327	182
	Water/Fe_2O_3	6.85×10^{-9}	8.864×10^{-7}	129	1303	207
	Water/Al_2O_3	6.12×10^{-9}	8.852×10^{-7}	145	1305	219
	Deionized water	5.27×10^{-9}	8.900×10^{-7}	169	1298	179

According to this equation by having an increase in nanoparticles density, more momentum can be transferred through the liquid phase; and consequently, a higher magnitude of micro-convections produces. Previous efforts declared that only two significant mechanisms including Brownian micro-convections and grazing effect (absorption of gas molecules by nanoparticles at the bubble-liquid interface and desorption of them into the liquid) can be involved during the gas absorption when a nanofluid is used as an absorbent [2–5,10,11,36]. For the absorption of CO_2, Brownian mechanism has a major impact on gas molecules transfer due to the fact that CO_2 molecules have not a very polar structure and asymmetric molecular configuration to produce high molecular charges (O=C=O) for being absorbed by nanoparticles surface charge; therefore, the Brownian mechanism indicates that water/Fe_2O_3 leads to a higher diffusivity of CO_2 because of the larger micro-convections. Consequently, the minimum value of CO_2 diffusivity in water/SiO_2 nanofluid could be observed due to the lower density and lower magnitude of micro-convections produced by SiO_2 nanoparticles.

On the other hands, due to the high polarity of SO_2 molecules and formation of its Lewis structure during the absorption process [37] (Figure 11), it can be easily absorbed by means of nanoparticles surficial charge, which they are at the vicinity of the bubble-liquid interface. In addition, it is reported from the previous researches that SiO_2 nanoparticles have a high value of surface charge due to the formation of silanol bonds (Si-O-H) at the nanoparticles surface [12], which has been confirmed by Zeta Potential test presented in this study. Therefore, the main mechanism for the absorption of SO_2 is attributed to grazing effect by means of nanoparticles at the bubble-liquid interface resulting a high diffusivity of SO_2 gas when water/SiO_2 nanofluid is used (Figure 11).

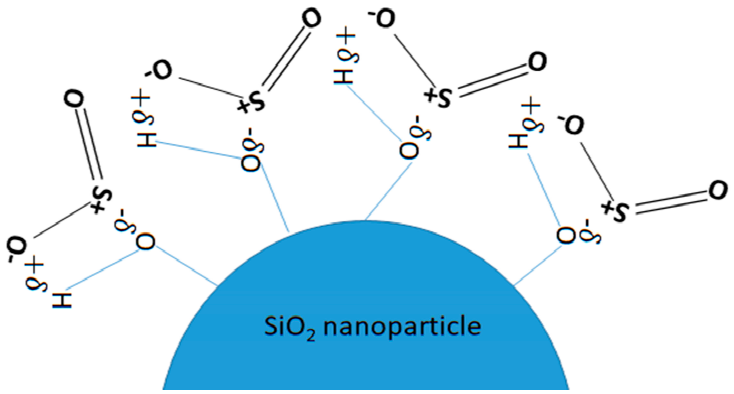

Figure 11. Schematic diagram of grazing effect of SiO_2 nanoparticles during the absorption of SO_2.

3.4. Correlation

Froessling [38] estimated the mas transfer of a raising bubble in a liquid by using Equation (13):

$$Sh = 0.6(Re)^{1/2}(Sc)^{1/3} \quad (13)$$

Equation (13) was found to be a suitable correlation for prediction of the absorption of different gases into wide ranges of liquids by means of single bubble absorber system [39]. In order to estimate *Sh* number for the gas absorption by nanofluids, other physical properties including dynamic viscosity, kinematic viscosity, and density of nanofluids were needed to obtain according to the following relations [40]:

$$\mu_{nf} = \mu_{bf}(1-\varphi)^{2.5} \tag{14}$$

$$\rho_{nf} = \varphi\rho_p + (1-\varphi)\,\rho_{bf} \tag{15}$$

$$\nu_{nf} = \mu_{nf}/\rho_{nf} \tag{16}$$

where φ is the volume fraction of oxides nanoparticles within the deionized water (can be obtained by using Equation (17) μ_{bf} is the dynamic viscosity of the deionized water, ρ_p is the bulk density of nanoparticles (presented in Table 1) and ρ_{bf} is the density of the deionized water (1000 kg/m^3).

$$\varphi(\%vol) = \frac{w(\%wt)}{w(\%wt) + \frac{\rho_p}{\rho_{bf}}(100 - w(\%wt))} \tag{17}$$

The values of *Re*, *Sc* and *Sh* can be calculated using the following equations:

$$Re_b = U_b d_b/\nu_{nf} \tag{18}$$

$$Sc_{nf} = \nu_{nf}/D_{nf} \tag{19}$$

$$Sh_{nf} = k_{L,nf}.d_b/D_{nf} \tag{20}$$

In these equations, U_b means the bubble rising velocity in the column that was approximately found to be 0.21 m/s for all the experiments. Additionally, d_b is the bubble diameter that was measured as 7 mm for all cases. Table 4 also presents the values of Re_b, *Sh* and *Sc* for the absorption of CO_2 and SO_2 by using the mentioned nanofluids.

According to Table 4 and Equation (18), the value of Reynolds number does not change significantly when either nanofluid or pure basefluid is applied during the absorption process by means of raising a single bubble absorber i.e., $\nu_{nf} \approx \nu_{bf}$. Therefore, it can be assumed that the Reynolds number has no significant effect on relative Sherwood number and this parameter is found to be just as a function of relative Schmidt number according to below:

$$\frac{Sh_{nf}}{Sh_{bf}} = K\left(\frac{Sc_{nf}}{Sc_{bf}}\right)^m \tag{21}$$

m and K were calculated by using a two-dimensional regression analysis over the experimental data shown in Figure 12. According to this figure, the following equation was obtained for the mentioned parameters with the R^2 = 0.9919. Equation (22) can predict the Sherwood number for various gas-nanofluid absorption systems at Re_b~1300, accurately:

$$\frac{Sh_{nf}}{Sh_{bf}} = 1.3643\left(\frac{Sc_{nf}}{Sc_{bf}}\right)^{0.6125} \qquad for\ Re_b \cong 1300 \tag{22}$$

It is mentioned that Sh_{bf} can be calculated by the Froessling equation (Equation (13)).

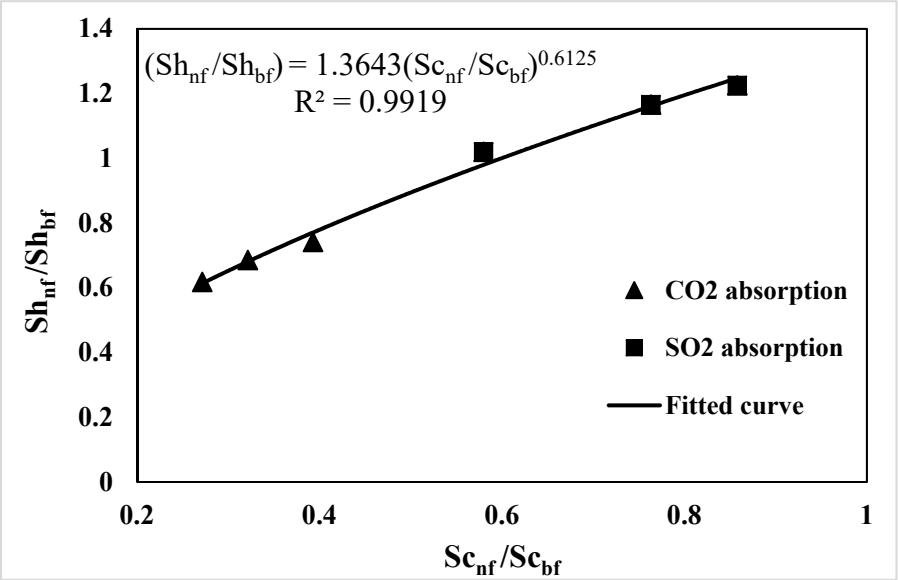

Figure 12. Effect of relative Schmidt number on relative experimental Sherwood number.

4. Conclusions

In this research, the absorption of SO_2 and CO_2 was elucidated by using a single-bubble column absorption setup into water based nanofluids containing SiO_2, Fe_2O_3 or Al_2O_3 nanoparticles. The results of this study clearly show that the aforementioned nanofluids have high stability since the zeta potential is lower than −45 mV. The results of TEM and DLS analysis also display that the average size of nanoparticles is within limit of 40–60 nm.

These results also declared that the maximum absorption of CO_2 and SO_2 could be obtained when water/SiO_2 or water/Fe_2O_3 nanofluid is utilized as an absorbent. Moreover, our findings also showed that the maximum relative absorption for SO_2 and CO_2 in the studied nanofluids in comparison to base fluid occurs when a water/Fe_2O_3 or water/SiO_2 nanofluid was used as the absorbent. Indeed, our results show that the type of gas molecules and nanoparticles determines the mechanism of mass transfer intensification of nanofluids. Therefore, both Brownian motion and grazing effect play crucial role for the increment of mass transfer in gas absorption by nanofluids. According to the type of gas and nanoparticles, the major mechanism can be distinguished.

In addition, mass transfer parameters incorporating diffusivity of gases into the oxides nanoparticles loaded in nanofluids, Sherwood number and Schmidt number were obtained. The results exhibit that the addition of nanoparticles (due to increment of Brownian momentum) increases diffusivity coefficient, and the maximum diffusivity for CO_2 and SO_2 absorption was obtained for water/Fe_2O_3 and water/SiO_2 nanofluids, respectively.

Finally, a new correlation is offered for the prediction of Sherwood number versus Schmidt number in gas-nanofluid systems (for Re_b about 1300) in which the experimental values are predicted with high accuracy.

Author Contributions: S.K.: Conceived and designed the analysis, Collected the data, Contributed data or analysis tools, Performed the analysis, Wrote the paper; F.E.: Conceived and designed the analysis, Contributed data or analysis tools, Performed the analysis, Wrote the paper; D.M.: Conceived and designed the analysis, Performed the analysis.

Funding: This research received no external funding.

Acknowledgments: The authors are grateful to the Shiraz University for supporting this research.

Conflicts of Interest: The authors declare no conflict of interest.

Nomenclature

N	Molar flux (mol/m^2 s)
C	Gas concentration at liquid bulk (mol/m^3)
C^*_{Obs}	The observed gas concentration at gas-liquid interface (mol/m^3)
V	Volume of nanofluid in the single bubble absorber (m^3)
n	Number of bubbles
τ	Average rising time for one bubble through the column (s)
r_0	Average radius of bubbles (m)
k_L	Mass transfer coefficient in liquid phase (m/s)
D	Diffusion coefficient (m^2/s)
δ	Diffusion layer thickness (mm)
s	Renewal surface factor (1/s)
Re_b	Reynolds number ($U_b d_b/\nu_{nf}$)
Sc	Schmidt number (ν_{nf}/D_{nf})
Sh	Sherwood number ($k_L d_b/D_{nf}$)
d_b	Diameter of bubbles raising through nanofluid (m)
φ	Volume fraction (%)
w	Mass fraction (%)
ρ	Density (kg/m^3)
v	Kinematic viscosity (m^2/s)
λ	Constant value for calculation of Brownian momentum transfer
R_{eff}	Relative absorption rate (N_{nf}/N_{bf})
M	HCl molarity (mol/lit)
λ	Constant value as a function of nanoparticles density, temperature, volume fraction, mean diameter, heat capacity, and Boltzmann constant.
Mo	Momentum that can be transferred by means of nanoparticle random motion
Subscript	
nf	Nanofluid
bf	Basefluid
p	Nanoparticles
B	Bubble

References

1. Nii, S.; Takeuchi, H. Removal of CO_2 and/or SO_2 from gas streams by a membrane absorption method. *Gas Sep. Purif.* **1994**, *8*, 107–114. [CrossRef]
2. Darvanjooghi, M.H.K.; Esfahany, M.N.; Esmaeili-Faraj, S.H. Investigation of the Effects of Nanoparticle Size on CO_2 Absorption by Silica-Water Nanofluid. *Sep. Purif. Technol.* **2017**. [CrossRef]
3. Darvanjooghi, M.H.K.; Pahlevaninezhad, M.; Abdollahi, A.; Davoodi, S.M. Investigation of the effect of magnetic field on mass transfer parameters of CO_2 absorption using Fe3O4-water nanofluid. *AIChE J.* **2017**, *63*, 2176–2186. [CrossRef]
4. Esmaeili-Faraj, S.H.; Nasr Esfahany, M.; Jafari-Asl, M.; Etesami, N. Hydrogen sulfide bubble absorption enhancement in water-based nanofluids. *Ind. Eng. Chem. Res.* **2014**, *53*, 16851–16858. [CrossRef]
5. Esmaeili-Faraj, S.H.; Nasr Esfahany, M. Absorption of hydrogen sulfide and carbon dioxide in water based nanofluids. *Ind. Eng. Chem. Res.* **2016**, *55*, 4682–4690. [CrossRef]
6. Kim, J.-K.; Jung, J.Y.; Kang, Y.T. Absorption performance enhancement by nano-particles and chemical surfactants in binary nanofluids. *Int. J. Refrig.* **2007**, *30*, 50–57. [CrossRef]
7. Baker, R.W. Future directions of membrane gas separation technology. *Ind. Eng. Chem. Res.* **2002**, *41*, 1393–1411. [CrossRef]
8. Richard, M.A.; Bénard, P.; Chahine, R. Gas adsorption process in activated carbon over a wide temperature range above the critical point. Part 1: Modified Dubinin-Astakhov model. *Adsorption* **2009**, *15*, 43–51. [CrossRef]
9. Whitman, W.G. The two film theory of gas absorption. *Int. J. Heat Mass Transf.* **1962**, *5*, 429–433. [CrossRef]

10. Ashrafmansouri, S.S.; Nasr Esfahany, M. Mass transfer into/from nanofluid drops in a spray liquid-liquid extraction column. *AIChE J.* **2016**, *62*, 852–860. [CrossRef]
11. Ashrafmansouri, S.S.; Esfahany, M.N. Mass transfer in nanofluids: A review. *Int. J. Therm. Sci.* **2014**, *82*, 84–99. [CrossRef]
12. Darvanjooghi, M.H.K.; Esfahany, M.N. Experimental investigation of the effect of nanoparticle size on thermal conductivity of in-situ prepared silica–ethanol nanofluid. *Int. Commun. Heat Mass Transf.* **2016**, *77*, 148–154. [CrossRef]
13. Chol, S. Enhancing thermal conductivity of fluids with nanoparticles. *ASME-Publ.-Fed* **1995**, *231*, 99–106.
14. Krishnamurthy, S.; Bhattacharya, P.; Phelan, P.; Prasher, R. Enhanced mass transport in nanofluids. *Nano Lett.* **2006**, *6*, 419–423. [CrossRef] [PubMed]
15. Kim, J.-K.; Jung, J.Y.; Kim, J.H.; Kim, M.-G.; Kashiwagi, T.; Kang, Y.T. The effect of chemical surfactants on the absorption performance during NH_3/H_2O bubble absorption process. *Int. J. Refrig.* **2006**, *29*, 170–177. [CrossRef]
16. Ma, X.; Su, F.; Chen, J.; Zhang, Y. Heat and mass transfer enhancement of the bubble absorption for a binary nanofluid. *J. Mech. Sci. Technol.* **2007**, *21*, 1813. [CrossRef]
17. Zhou, M.; Cai, W.F.; Xu, C.J. A new way of enhancing transport process–The hybrid process accompanied by ultrafine particles. *Korean J. Chem. Eng.* **2003**, *20*, 347–353. [CrossRef]
18. Kang, Y.T.; Lee, J.-K.; Kim, B.-C. Absorption heat transfer enhancement in binary nanofluids. In *International Congress of Refrigeration*; Curran Associates, Inc.: Beijing, China, 2007.
19. Yang, L.; Du, K.; Niu, X.F.; Cheng, B.; Jiang, Y.F. Experimental study on enhancement of ammonia–water falling film absorption by adding nano-particles. *Int. J. Refrig.* **2011**, *34*, 640–647. [CrossRef]
20. Attari, H.; Derakhshanfard, F.; Darvanjooghi, M.H.K. Effect of temperature and mass fraction on viscosity of crude oil-based nanofluids containing oxide nanoparticles. *Int. Commun. Heat Mass Transf.* **2017**, *82*, 103–113. [CrossRef]
21. Heris, S.Z.; Etemad, S.G.; Esfahany, M.N. Experimental investigation of oxide nanofluids laminar flow convective heat transfer. *Int. Commun. Heat Mass Transf.* **2006**, *33*, 529–535. [CrossRef]
22. Kang, Y.T.; Kim, H.J.; Lee, K.I. Heat and mass transfer enhancement of binary nanofluids for H_2O/LiBr falling film absorption process. *Int. J. Refrig.* **2008**, *31*, 850–856. [CrossRef]
23. Wang, X.-Q.; Mujumdar, A.S. Heat transfer characteristics of nanofluids: A review. *Int. J. Therm. Sci.* **2007**, *46*, 1–19. [CrossRef]
24. Jung, J.-Y.; Lee, J.W.; Kang, Y.T. CO_2 absorption characteristics of nanoparticle suspensions in methanol. *J. Mech. Sci. Technol.* **2012**, *26*, 2285–2290. [CrossRef]
25. Andrade, Â.L.; Fabris, J.D.; Ardisson, J.D.; Valente, M.A.; Ferreira, J.M. Effect of tetramethylammonium hydroxide on nucleation, surface modification and growth of magnetic nanoparticles. *J. Nanomater.* **2012**, *2012*, 15. [CrossRef]
26. Andrade, Â.L.; Souza, D.M.; Pereira, M.C.; Fabris, J.D.; Domingues, R.Z. pH effect on the synthesis of magnetite nanoparticles by the chemical reduction-precipitation method. *Quim. Nova* **2010**, *33*, 524–527. [CrossRef]
27. Davoodi, S.M.; Sadeghi, M.; Naghsh, M.; Moheb, A. Olefin–paraffin separation performance of polyimide Matrimid®/silica nanocomposite membranes. *RSC Adv.* **2016**, *6*, 23746–23759. [CrossRef]
28. Terraglio, F.P.; Manganelli, R.M. The absorption of atmospheric sulfur dioxide by water solutions. *J. Air Pollut. Control Assoc.* **1967**, *17*, 403–406. [CrossRef]
29. Zhao, B.; Wang, J.; Yang, W.; Jin, Y. Gas–liquid mass transfer in slurry bubble systems: I. Mathematical modeling based on a single bubble mechanism. *Chem. Eng. J.* **2003**, *96*, 23–27. [CrossRef]
30. Skoog, D.A.; West, D.M. *Fundamentals of Analytical Chemistry*; Thomson Brooks/Cole: Pacific Grove, CA, USA, 2004.
31. Teng, T.-P.; Hung, Y.-H.; Teng, T.-C.; Mo, H.-E.; Hsu, H.-G. The effect of alumina/water nanofluid particle size on thermal conductivity. *Appl. Therm. Eng.* **2010**, *30*, 2213–2218. [CrossRef]
32. Vijayakumar, R.; Koltypin, Y.; Felner, I.; Gedanken, A. Sonochemical synthesis and characterization of pure nanometer-sized Fe_3O_4 particles. *Mater. Sci. Eng. A* **2000**, *286*, 101–105. [CrossRef]
33. áO'Brien, R.W. Electroacoustic studies of moderately concentrated colloidal suspensions. *Faraday Discuss. Chem. Soc.* **1990**, *90*, 301–312. [CrossRef]

34. Faraji, M.; Yamini, Y.; Rezaee, M. Magnetic nanoparticles: Synthesis, stabilization, functionalization, characterization, and applications. *J. Iran. Chem. Soc.* **2010**, *7*, 1–37. [CrossRef]
35. Kim, W.-G.; Kang, H.U.; Jung, K.-M.; Kim, S.H. Synthesis of silica nanofluid and application to CO_2 absorption. *Sep. Sci. Technol.* **2008**, *43*, 3036–3055. [CrossRef]
36. Koo, J.; Kleinstreuer, C. Impact analysis of nanoparticle motion mechanisms on the thermal conductivity of nanofluids. *Int. Commun. Heat Mass Transf.* **2005**, *32*, 1111–1118. [CrossRef]
37. Purser, G.H. Lewis structures are models for predicting molecular structure, not electronic structure. *J. Chem. Educ.* **1999**, *76*, 1013. [CrossRef]
38. Vasconcelos, J.M.; Orvalho, S.P.; Alves, S.S. Gas–liquid mass transfer to single bubbles: Effect of surface contamination. *AIChE J.* **2002**, *48*, 1145–1154. [CrossRef]
39. Calderbank, P.; Lochiel, A. Mass transfer coefficients, velocities and shapes of carbon dioxide bubbles in free rise through distilled water. *Chem. Eng. Sci.* **1964**, *19*, 485–503. [CrossRef]
40. Mishra, P.C.; Mukherjee, S.; Nayak, S.K.; Panda, A. A brief review on viscosity of nanofluids. *Int. Nano Lett.* **2014**, *4*, 109–120. [CrossRef]